PREDICTION OF FATIGUE CRACK-GROWTH PATTERNS AND LIVES IN THREE-DIMENSIONAL CRACKED BODIES

J. C. Newman, Jr.* and I. S. Raju**

*NASA Langley Research Center, Mail Stop 188E, Hampton, VA 23665, USA
**Vigyan Research Associates, Inc., 28 Research Drive, Hampton, VA 23666, USA

ABSTRACT

Fatigue crack-growth patterns and lives for surface cracks, surface cracks at holes, and corner cracks at holes in three-dimensional bodies were predicted using linear-elastic fracture mechanics concepts that were modified to account for crack-closure behavior. The predictions were made by using stress-intensity factor equations for these crack configurations and the fatigue crack-growth (ΔK against rate) relationship for the material of interest. The crack configurations were subjected to constant-amplitude fatigue loading under either remote tension or bending loads. The predicted crack-growth patterns and crack-growth lives for aluminum alloys agreed well with test data from the literature.

KEYWORDS

Cracks; surface cracks; corner cracks; crack propagation; fatigue (materials); stress-intensity factors; crack closure; fracture.

INTRODUCTION

The requirement for lightweight aerospace structures leads to high design stresses. High stresses can produce cracks early in the fatigue life of these structural components. Such cracks grow under flight loading and may, ultimately, lead to catastrophic failure. A comprehensive review of aerospace structural failures, completed by the U.S. Air Force (Gran and others, 1971), showed that most failures originate as surface cracks, corner cracks, or cracks at fastener holes. For the structural design to be damage tolerant, accurate methods to predict crack-growth rates and fracture strengths for these crack configurations are needed. Consequently, during the past decade, much research has been directed toward developing the stress-intensity factor solutions for these crack configurations. Based on extensive numerical analyses of Raju and Newman (1979a, 1979b), empirical stress-intensity factor equations for elliptical, semi-elliptical, and quarter-elliptical cracks in three-dimensional bodies were developed by Newman and Raju (1979, 1983).

In this paper, the stress-intensity factor equations were used to predict fatigue crack-growth patterns and lives for surface cracks, surface cracks at holes, and corner cracks at holes. The bodies containing these crack configurations were subjected to constant-amplitude fatigue loading under either remote tension or bending loads. The predicted crack-growth patterns and lives of several aluminum alloys are compared with test data from the literature.

CRACK-GROWTH ANALYSIS

In this section, the configurations analyzed and the procedure used for fatigue crack-growth predictions are presented. The crack-growth predictions are based on linear-elastic fracture mechanics concepts that have been modified to include crack-closure effects. The procedure, however, can only be used for constant-amplitude loading.

Configurations and Loading

Three crack configurations are commonly encountered in aerospace structural components. These configurations are: (1) the surface crack, (2) the surface crack at a hole, and (3) the corner crack at a hole. For cracks that are elliptical, semi-elliptical, or quarter-elliptical in shape, stress-intensity factor equations were developed by Newman and Raju (1979, 1983). These equations cover a wide range of configuration parameters. They were used together with appropriate crack-growth rate (ΔK against rate) relationships for particular materials to predict the growth of these cracks under cyclic loading.

The cracked bodies were subjected to constant-amplitude cyclic loading that produced a maximum remote stress of S_{max} and a minimum remote stress of S_{min}. The stress ratio (R) is defined as S_{min}/S_{max}. For the surface crack configuration (Fig. 1), remote tension (S_t) and bending (S_b) stresses were considered. For the other crack configurations, Figs. 2(a) and 2(b), only remote tensile stress was considered.

Procedure

The procedure used to predict crack-growth patterns for the surface-cracked plate is presented here. The same procedure was used for the other crack configurations considered.

For the surface-cracked plate, the stress-intensity factor equations developed by Newman and Raju (1979) give the stress-intensity factor at any location along the crack front. The cracks, however, were assumed to grow in semi-elliptical shapes with semi-axes of a and c, so only the predicted growths at the maximum depth point A and the surface point B (see Fig. 1) were needed to define the crack shape as the crack grew.

Crack-growth rate relationship. The crack-growth rates were calculated by assuming that the Elber (1971) relationship between the crack-growth rate and the effective stress-intensity factor range (ΔK_{eff}) is obeyed independently at points A and B. Thus, the rate at point A is given by

$$\frac{da}{dN} = \overline{C}_i \left(\Delta K_{eff} \right)_A^{n_i} = \overline{C}_i \left(U_A \, \Delta K_A \right)^{n_i} \qquad (1)$$

and at point B is given by

$$\frac{dc}{dN} = \overline{C}_i \left(\Delta K_{eff} \right)_B^{n_i} = \overline{C}_i \left(U_B \, \Delta K_B \right)^{n_i} \qquad (2)$$

where ΔK and ΔK_{eff} are the full and effective stress-intensity factor ranges, respectively, n_i is the crack-growth power, and $\overline{C}_i$ is the crack-growth coefficient. The factors U_A and U_B are the crack-closure factors (Elber, 1971). Defining C_i as $\overline{C}_i U_A^{n_i}$, Equations (1) and (2) are rewritten as

$$\frac{da}{dN} = C_i \left(\Delta K_A \right)^{n_i} \qquad (3)$$

and

$$\frac{dc}{dN} = C_i \left(\frac{U_B}{U_A} \, \Delta K_B \right)^{n_i} = C_i \left(\beta_R \, \Delta K_B \right)^{n_i} \qquad (4)$$

The determination of β_R will be discussed later.

For tests with a constant R-ratio, a plot of ΔK against crack-growth rate does not follow a straight line on a log-log plot as suggested by Equations (3) and (4). Therefore, to better approximate the crack-growth rate relationship, the ΔK against crack-growth rate curve was divided into a number of linear segments. The number of segments varied from 3 to 5, that is, $i = 1$ to 3, 4, or 5. Thus, C_i and n_i in Equations (3) and (4) are functions of segment number as well as material and R-ratio. In this paper C_i and n_i were determined from crack-growth rate data from either compact or center-crack tension specimens at the desired R-ratio.

Determination of crack-closure factor ratio (β_R). Earlier studies have shown that crack-growth predictions of semi-elliptical surface cracks cannot be solely predicted by stress-intensity factor ranges alone (Newman and Raju, 1979). For $R = 0$ loading, small semicircular surface cracks tend to grow in a self-similar fashion, although the stress-intensity factor at point B (see Fig. 1) is about 10 percent higher than that at point A. To account for this difference, Newman and Raju (1979) used a β_R factor of 0.9, and Jolles and Tortoriello (1983a) used a factor of 0.911. As previously derived, this factor is related to crack-closure differences at points A and B.

The β_R factor also appears to be a function of the R-ratio. Jolles and Tortoriello (1983b) tested surface-cracked 2024-T351 aluminum alloy specimens and noted that for R-ratios greater than about 0.7, the cracks are always fully open and the stress-intensity factor range is fully effective. For $0 \leq R \leq 0.5$, the test results of Jolles and Tortoriello (1983b) suggest that crack closure occurs all along the crack front, but that the crack-closure factor (U) differs at points A and B. Their factors U_B and U_A were given by

$$U_B = 0.707 + 0.408R \qquad (5)$$

and

$$U_A = 1.098U_B \qquad (6)$$

for $0 \leq R \leq 0.5$. In the range $0.5 < R \leq 0.7$, crack closure should not occur under plane-strain conditions at point A and, therefore, U_A should be equal to unity. Closure should occur under plane-stress conditions at point B, and U_B is given by Equation (5). For $R > 0.7$, both U_A and U_B are equal to unity. (Analytical calculations by Newman (1981) have also shown that under plane-strain conditions cracks are always fully open for $R \geq 0.5$, and that under plane-stress conditions cracks are always fully open for $R \geq 0.7$.)

To determine β_R, the ratio of U_B to U_A from Equations (5) and (6) was computed for discrete values of R and a smooth function was fitted to these results. The test data from Jolles and Tortoriello (1983b) and the fitted curve are shown in Fig. 3. The crack-closure factor ratio is

$$\beta_R = 0.9 + 0.2R^2 - 0.1R^4 \qquad (7)$$

for $R \geq 0$, and β_R is assumed to be 0.9 for $R < 0$. For negative R-ratios, the 0.9 factor seems reasonable on the basis of analytical calculations by Newman (1981).

Crack-growth prediction. To predict crack growth of a surface crack in a specimen subjected to constant-amplitude loading at a particular R-ratio, the C_i and n_i in Equations (3) and (4) are obtained from growth data for that same R-ratio. The crack extension from the initial crack length to failure ($c_f - c_o$) is divided into a large number of equal increments Δc. Within each increment of crack growth, Δc, the crack was assumed to grow at a constant rate. The stress-intensity factor range, ΔK_B, was computed from the stress-intensity factor equation (Newman and Raju, 1979) using the current crack length c, crack depth a, and applied load. The growth rate dc/dN was calculated from Equation (4). Because Δc is known, the number of incremental cycles was given by $\Delta N = \Delta c/(dc/dn)$. Next, the stress-intensity factor range at point A, ΔK_A, was computed. The corresponding rate, da/dN, was calculated from Equation (3). The growth increment Δa was then computed by $\Delta a = (da/dN) \Delta N$. The crack now has a semi-elliptical shape with semi-axes of $(a + \Delta a)$ and $(c + \Delta c)$. Using the new values of a and c, the above procedure was repeated until the crack depth reached the plate thickness. At this point (a = t), the surface crack was assumed to change instantaneously into a through-the-thickness crack of half-length c. Thereafter, the appropriate stress-intensity factor equation for a through crack was used to compute growth rates.

The above procedure was used to predict the growth of surface cracks. For the other configurations, a similar procedure was used, except that the β_R factor was applied at all points where a crack intersects a free surface. For example, for a surface crack at a hole (Fig. 2(a)), the β_R factor is applied at point A only. In contrast, for a corner crack at a hole (Fig. 2(b)), the β_R factor is applied at both points A and B.

RESULTS AND DISCUSSION

The crack-growth analysis was used to predict the fatigue crack-growth patterns for three crack configurations. The first was a surface crack in a plate subjected to remote tension and bending loads. The second and third were a surface crack and a corner crack at a circular hole in a plate subjected to remote tension. The predicted crack-growth patterns are compared with test results from the literature. In all of the figures, the initial crack configuration is shown by solid symbols, the experimental data are shown by open symbols, and the predictions are shown by curves.

Surface Crack in a Plate

Crack-growth patterns under tension. Figure 4 shows the experimental and predicted fatigue crack-growth patterns for surface cracks in 2024-T351 aluminum alloy specimens subjected to remote tension loading with R-ratios ranging from 0.1 to 0.75. The test results were taken from Jolles and Tortoriello (1983b). The predicted growth patterns (curves) agree well with the few data available. They show how the R-ratio affects the growth patterns. The high R-ratio tests show a more rapid change in crack shape than do the low R-ratio tests.

The crack-growth analysis has also been successfully applied to surface cracks in a titanium alloy, a nickel steel, and other aluminum alloys by Newman and Raju (1979).

Crack-growth patterns under bending. Figure 5 shows the experimental and predicted fatigue crack-growth patterns for surface cracks in 2014-T651 aluminum alloy plates subjected to cantilever bending with R = 0.1. The a/c ratio is plotted as a function of the a/t ratio. Each open symbol in the figure represents a test (Corn, 1971) on a separate specimen. The specimens were cycled under constant-amplitude loading and then statically pulled to failure.

The predicted fatigue crack-growth patterns agree well with the data in Fig. 5. The predicted results show that the cracks tended to approach a common propagation pattern, as pointed out by Corn (1971).

Crack-growth life under tension. Figure 6 shows experimental and predicted crack-length-against-cycles for a surface crack in a 2219-T851 aluminum alloy plate subjected to remote tension loading with an R-ratio of 0.05. The data were taken from Chang (1979). The square symbols show crack growth in the depth direction, a, and the circular symbols show growth along the free surface, c.

The crack-growth rate constants, C_i and n_i, were obtained from compact specimens tested at the same R-ratio (Chang, 1979). The curves in Fig. 6 show predicted depth and surface growth. The predictions agree well with show predicted depth and surface growth. The predictions agree well with the data. The predicted number of cycles for the crack depth, a, to reach the thickness of the plate, t, exceeds the test results by only 10 percent.

Surface Crack at a Hole in a Plate

Crack-growth patterns. Figure 7 shows experimental and predicted crack shapes for a surface crack located at the plate mid-thickness on the bore of a circular hole in a 7075-T651 aluminum alloy plate subjected to remote

tension loading. The test results were taken from McGee and Hsu (1981). The maximum stress level (S_{max}) in the fatigue test was 103 MPa and the R-ratio was 0.1. The starter crack had an a/c ratio of 2.43 and an a/t ratio of 0.2. A high R-ratio (R = 0.85) loading with the same S_{max} was used to mark the fatigue surface. After the specimen was broken, the crack lengths a and c were measured from the marker bands on enlarged photographs of the fatigue surfaces.

The predicted crack shapes were calculated by using C_i and n_i values obtained from center-crack tension specimens tested at the same R-ratio. The predicted result is shown as the curve in Fig. 7. Crack growth, from the test and analysis, is much faster at the deepest point (c) than at the hole boundary for the initial crack shape considered here. The crack shape appears to stabilize at an a/c ratio of about 1.5.

Crack-growth life. Figure 8 shows experimental and predicted crack-length-against-cycles for a surface crack at a hole. The predicted results agreed well with the experimental data. The predicted number of cycles for the crack depth, a, to reach the plate thickness was only about 5 percent higher than the experimental results.

Corner Crack at a Hole in a Plate

Experimental and predicted crack-growth patterns and crack-growth lives of a corner crack emanating from a hole are compared for two different materials, 7075-T651 and 7050-T73 aluminum alloy.

Crack-growth patterns and lives in 7075-T651 aluminum alloy. Figure 9 shows the ratio of predicted-to-experimental crack depth for different R-ratios for a corner crack growing from a hole in a 7075-T651 aluminum alloy plate subjected to remote tension. The tests are from J. Rudd (Wright-Patterson Air Force Base). The tests were conducted under constant-amplitude loading at S_{max} levels of 103 and 130 MPa and at several R-ratios. The starter crack was grown from a very small electro-discharge-machine notch. The initial a and c values were approximately 1.3 and 2 mm in length, respectively. When the crack length, c, reached a value of 3 mm, the crack depth along the hole, a, was measured.

Predictions of crack depth, a, were made for various R-ratios and stress levels used in the tests. The ratios of predicted-to-experimental crack depth (a_P/a_T) are plotted against the R-ratio in Fig. 9. The solid horizontal line represents perfect correlation between the predictions and tests. The predicted crack depths at c = 3 mm were within 10 percent of the experimental depths in all cases. In Fig. 10, the ratios of predicted cycles (N_P) to test cycles (N_T) when the crack depth reaches the plate thickness (a = t) are also plotted against the R-ratio. The predicted lives were within about 30 percent of the test lives.

Crack-growth patterns and lives in 7050-T73 aluminum alloy. Figure 11 shows experimental and predicted crack dimensions for a corner crack growing at a hole in a 7050-T73 aluminum alloy specimen subjected to tension. The data are from Hsu, McGee, and Aberson (1978). An electro-discharge-machine process was used to introduce an initial notch at the edge of the hole. The specimen was subjected to constant-amplitude loading with a maximum stress level of 103 MPa at a stress ratio of 0.1. The fatigue surface was marked using the marker-band technique as described by McGee and Hsu (1981).

The initial notch had an a/t ratio of 0.12 and a c/t ratio of 0.26. Starting with the initial crack shape, the fatigue crack dimensions were predicted during crack growth. In Fig. 11, the predicted crack shape is compared to test results at two stages of the test. The predicted shape was assumed to be quarter-elliptical in shape, with semi-major and semi-minor axes equal to the a/t and c/t values. Good agreement was observed between test and prediction when the a/t value was small, but only fair agreement was observed when the a/t value became large.

The test data showed slower crack growth in the c-direction than the prediction. This may have been caused by residual stresses in the material near the free surface.

Figure 12 shows experimental and predicted crack-length-against-cycles for the corner-crack configuration. The predicted results in the c-direction agreed well with the experimental results. At breakthrough (a = t), the predicted number of cycles for crack depth (a) was about 30 percent higher than the experimental results.

After the crack depth (a) reached the plate thickness, predictions of crack growth in the c-direction were made using the stress-intensity factor solution for a through crack emanating from a circular hole (Tada, Paris, and Irwin, 1973). Figure 12 shows excellent correlation between the predicted and experimental results for the through-the-thickness configuration.

CONCLUDING REMARKS

Fatigue crack-growth patterns and lives for surface cracks, surface cracks at holes, and corner cracks at holes in three-dimensional crack bodies were predicted using modified linear-elastic fracture mechanics concepts. The cracked specimens were subjected to either remote tension or bending loads. Constant-amplitude cycling was applied with stress ratio (R) varying from -0.5 to 0.75. The stress-intensity factor equations developed by Newman and Raju for these configurations were used in the predictions. The crack-growth rate relationship, dc/dN against ΔK, for each material of interest was obtained from either center-crack tension or compact specimens.

The cracks were assumed to grow in semi-elliptical or quarter-elliptical shapes. Consequently, only the stress-intensity factor ranges at the maximum depth point and at the tip of the crack at the surface needed to be considered.

A crack-closure factor ratio, which is a function of the R-ratio, was developed and used to account for the variation in crack-closure behavior along the crack front. Effective stress-intensity factors were lower at locations where the crack intersected free surfaces than at interior locations.

Predicted fatigue crack-growth patterns and lives for aluminum alloys were compared with test data taken from the literature. In all cases, the predicted trends (patterns and life) followed the test data. For most cases, the predicted number of cycles for a crack to grow to the plate thickness was within ±30 percent of the experimental results.

REFERENCES

Chang, J. B. (1979). Assessment of the sensitivity of crack growth rate constants to predictive accuracy of part-through crack fatigue life predictions. In J. B. Chang (Ed.), Part-Through Crack Fatigue Life Prediction, ASTM STP 687. American Society for Testing and Materials, Philadelphia, 156-167.

Corn, D. L. (1971). A study of cracking techniques for obtaining partial thickness cracks of pre-selected depths and shapes. Engng Fracture Mechs., 3, 45-52.

Elber, W. (1971). The significance of fatigue crack closure. In Damage Tolerance in Aircraft Structures, ASTM STP 486. American Society for Testing and Materials, Philadelphia, 230-242.

Gran, R. J., F. D. Orazio, P. C. Paris, G. R. Irwin, and R. H. Hertzberg (1971). Investigation and analysis development of early life aircraft structural failures. AFFDL-TR-70-149, U.S. Air Force Flight Dynamics Laboratory.

Hsu, T. M., W. M. McGee, and J. A. Aberson (1978). Extended study of flaw growth at fastener holes. AFFDL-TR-77-83, U.S. Air Force Flight Dynamics Laboratory.

Jolles, M., and V. Tortoriello (1983a). Geometry variations during fatigue growth of surface flaws. In J. C. Lewis and G. Sines (Eds.), Fracture Mechanics: Fourteenth Symposium--Volume I: Theory and Analysis, ASTM STP 791. American Society for Testing and Materials, Philadelphia, I-297-I-307.

Jolles, M., and V. Tortoriello (1983b). Effects of constraint variation on the fatigue growth of surface flaws. Presented at the Fifteenth National Symposium on Fracture Mechanics, College Park, MD.

McGee, W. M., and T. M. Hsu (1981). Growth characteristics for fatigue cracks embedded in fastener hole walls. Engng Fracture Mechs., 14, 595-606.

Newman, J. C., Jr., and I. S. Raju (1979). Analysis of surface cracks in finite plates under tension and bending loads. NASA TP-1578, National Aeronautics and Space Administration.

Newman, J. C., Jr. (1981). A crack-closure model for predicting fatigue crack growth under aircraft spectrum loading. In J. B. Chang and C. M. Hudson (Eds.), Methods and Models for Predicting Fatigue Crack Growth under Random Loading, ASTM STP 748. American Society for Testing and Materials, Philadelphia, 53-84.

Newman, J. C., Jr., and I. S. Raju (1983). Stress-intensity factor equations for cracks in three-dimensional finite bodies. In J. C. Lewis and G. Sines (Eds.), Fracture Mechanics: Fourteenth Symposium--Volume I: Theory and Analysis, ASTM STP 791. American Society for Testing and Materials, Philadelphia, I-238-I-265.

Raju, I. S., and J. C. Newman, Jr. (1979a). Stress-intensity factors for a wide range of semi-elliptical surface cracks in finite-thickness plates. Engng Fracture Mechs., 11, 817-829.

Raju, I. S., and J. C. Newman, Jr. (1979b). Stress-intensity factors for two symmetric corner cracks. In C. W. Smith (Ed.), Fracture Mechanics, ASTM STP 677. American Society for Testing and Materials, Philadelphia, 411-430.

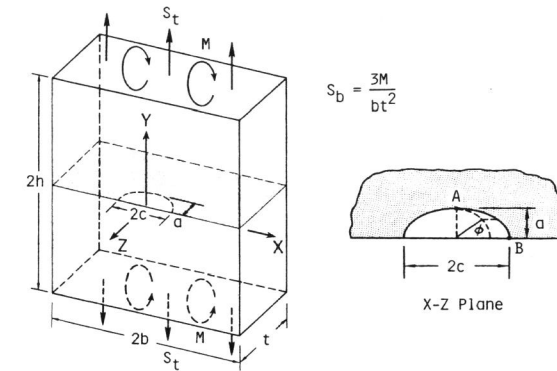Tada, H., P. C. Paris, and G. R. Irwin (1973). The Stress Analysis of Cracks Handbook. Del Research Corporation.

Fig. 1. Surface crack in a plate.

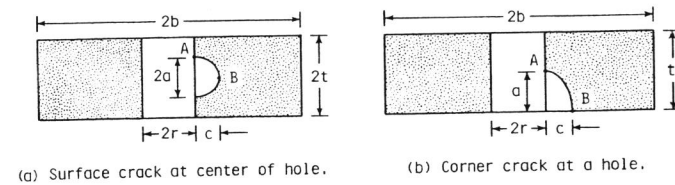(a) Surface crack at center of hole. (b) Corner crack at a hole.

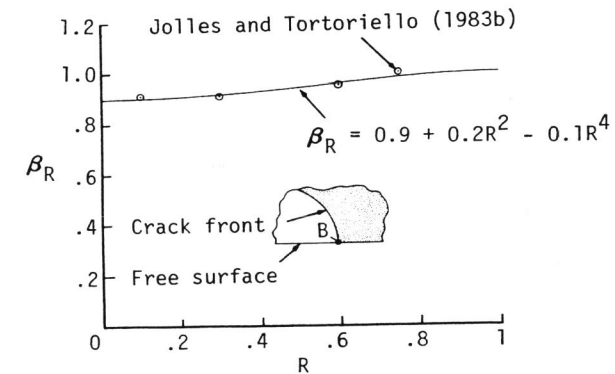Fig. 2. Surface crack and corner crack at a circular hole.

Fig. 3. Crack-closure factor ratio as a function of stress ratio.
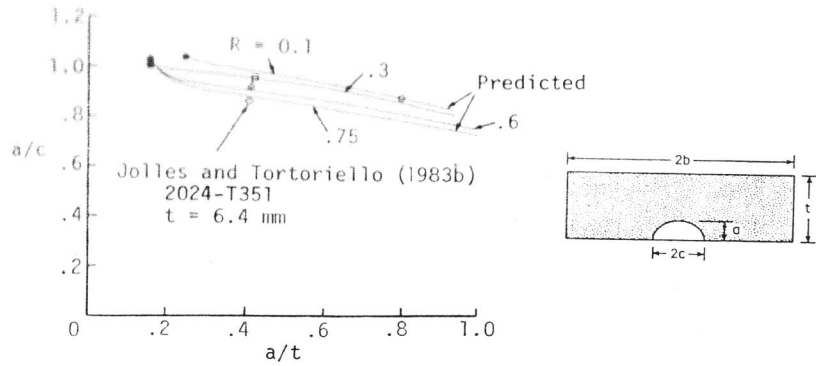
Fig. 4. Experimental and predicted fatigue crack-growth patterns for a surface crack under tension.
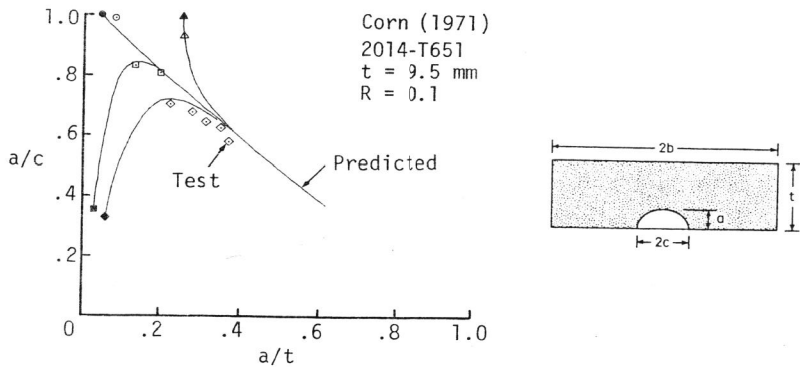

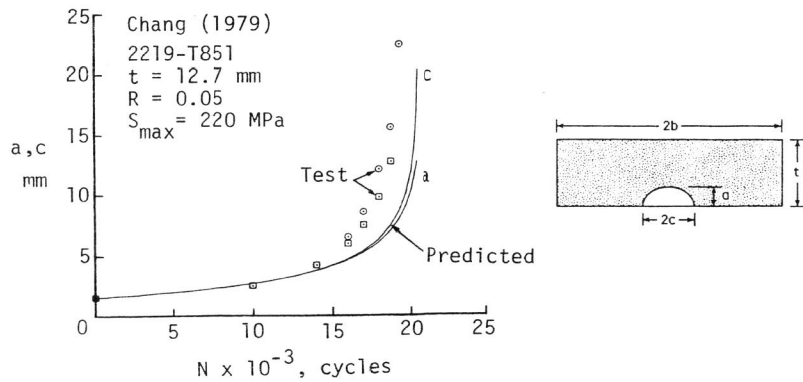Fig. 5. Experimental and predicted fatigue crack-growth patterns for a surface crack under bending.

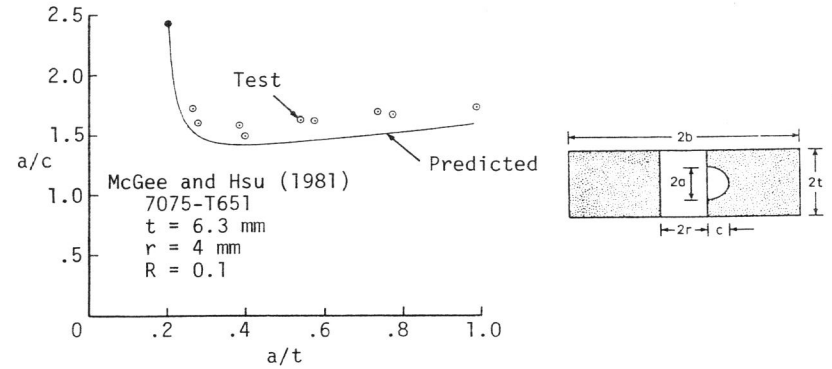Fig. 6. Experimental and predicted fatigue crack growth for a surface crack under tension.

Fig. 7. Experimental and predicted fatigue crack-growth patterns for a surface crack at a hole under tension.
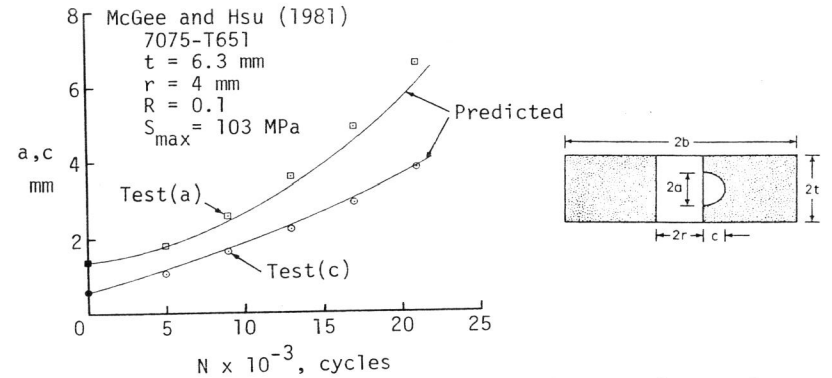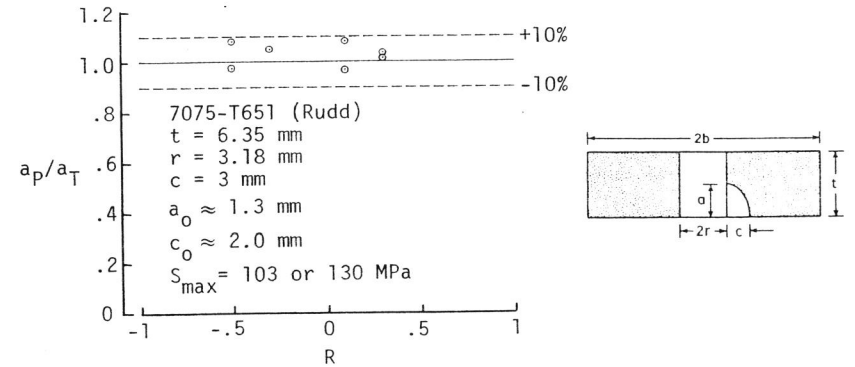

Fig. 8. Experimental and predicted fatigue crack growth for a surface crack at a hole under tension.

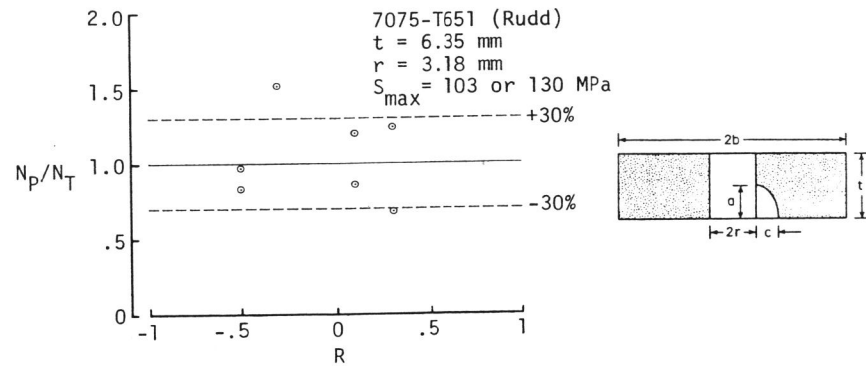Fig. 9. Ratio of predicted-to-experimental crack depth for a corner crack at a hole under tension.

Fig. 10. Ratio of predicted-to-experimental cycles to breakthrough
(a = t) for a corner crack at a hole under tension.
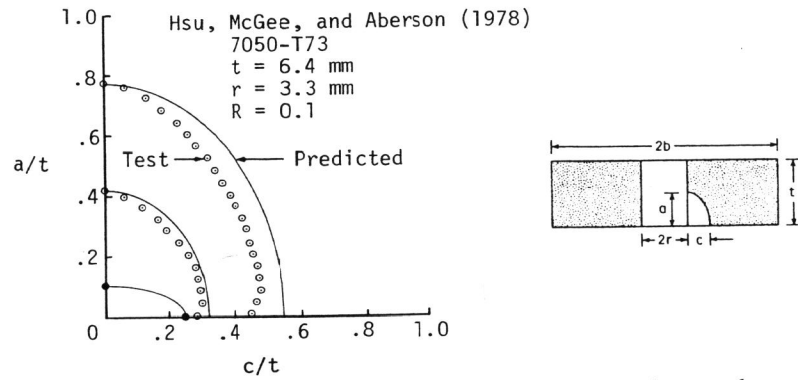

Fig. 11. Experimental and predicted fatigue crack-growth
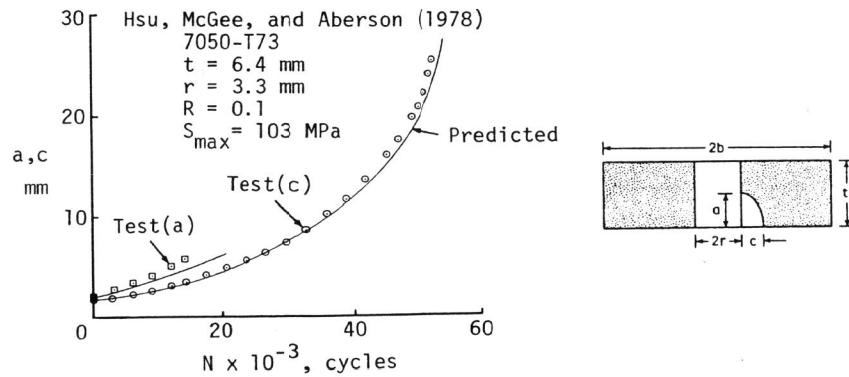patterns for a corner crack at a hole under tension.

Fig. 12. Experimental and predicted fatigue crack growth
for a corner crack at a hole under tension.